

Exploring the Limits in Individual Pitch Control

S.K. Kanev

T.G. van Engelen

This report has been presented at the European Wind Energy Conference 2009, Marseille, France, 16-19 March 2009

March 2009

ECN-M--09-053

Exploring the Limits in Individual Pitch Control

Stoyan Kanev
ECN Wind Energy,
P.O. Box 1, 1755ZG Petten, The Netherlands
kanev@ecn.nl

Tim van Engelen ECN Wind Energy, P.O. Box 1, 1755ZG Petten, The Netherlands vanengelen@ecn.nl

1 Abstract

Individual pitch control (IPC) is an advanced wind turbine control method for fatigue load reduction. The conventional IPC algorithm (cyclic pitch control) aims at achieving 1p blade load reduction by mitigating the static rotor tilt and yaw moments. Besides these existing IPC methods, this paper presents a novel application of IPC: rotor balancing. Imperfections in the blades lead to aerodynamic and/or mass unbalance that result in variations at the rotational frequency 1p in the rotor tilt and yaw moments. The new IPC algorithm compensates for such rotor unbalance by adding quasi-steady offsets to the blade pitch angles. As a second contribution, an "anti-windup" IPC implementation is proposed for dealing with blade actuator limitations. Detailed nonlinear simulations are used to validate the proposed IPC algorithms.

Keywords: wind turbine control, individual pitch control, load reduction, actuator limitations, anti-windup.

2 Introduction

Modern wind turbines have the possibility of individually pitching the blades, opening the road towards the use of advanced individual pitch control (IPC) algorithms for achieving fatigue load reduction. Different effects (e.g. tower shadow, wind shear, yawmisalignment, and rotational wind field sampling) result in blade loads at the rotational frequency (1p) and multiples of it (1p, 2p, 3p, etc.). Blade load reduction by IPC can be achieved by using additional measurements, such as blade root bending moments, shaft bending moments, or tower-top bending moments measured at the yaw bearing. Using blade root bending moments measurements with which modern wind turbines are often equipped, gives rise to a periodic system which complicates the IPC design. This problem can fortunately be circumvented by transforming all quantities (pitch angles, blade moments, etc.), defined on the rotating reference frame, to the fixed frame by using the so-called Coleman transformation [10], which results in a linear time-invariant (LTI) model. The blade root flapwise bending moments, for instance, are transformed into rotor tilt and yaw moments, which are used by the IPC to compute tilt-oriented and yaw-oriented pitch signals. Thus the Coleman transformation makes the application of well-developed control theory for LTI systems to the IPC problem possible. In addition, the treatment in fixed-frame coordinates allows for the decoupling of the collective pitch control (CPC) design from the IPC design because of negligible interaction in the relevant frequencies.

The use of IPC for 1p blade load reduction has received attention in the literature lately [3, 4, 1], where the conventional approach aims at static rotor tilt and yaw moments reduction by using integral-type control. These rotor moments can either be measured directly (e.g. at the yaw bearing), or can be reconstructed from measured blade root (or shaft) bending moments. The IPC computes so-called tilt and yaw oriented blade pitch signals which are then demodulated by the inverse Coleman transformation into three individual blade pitch angles. In this way, the IPC adds almost-periodical blade pitch angle variations at the 1p frequency to the collective blade pitch angle. Modern control can be used for the synthesis of more complex IPC controllers for 2p (and higher) blade load reduction [3, 4, 7, 5].

Differences in the profile properties of rotor blades, as well as in the blade pitch setting angles, during assemblage lead to aerodynamic unbalance. Moreover, inaccuracies in the mass properties during assemblage lead to mass unbalance. During operation in cold climates, ice formation can have similar effects. Neglecting such unbalance can severely degrade the performance of the IPC load reduction algorithm. A novel IPC algorithm is proposed that achieves rotor balancing by pitching the blades to some quasi-static pitch angles (different for each blade) in such a way, that the static shaft loads are mitigated.

Bringing modern IPC algorithms into practice necessitates the consideration of the actuator limitations, expressed as position, velocity and acceleration constraints on the blade pitch signals. Due to the intrinsic integral type of the IPC algorithms, anti-windup schemes must be implemented to avoid instability. As a second contribution of the paper, anti-windup IPC scheme is developed. To this end, the original pitch actuator limits are transformed into constraints on the

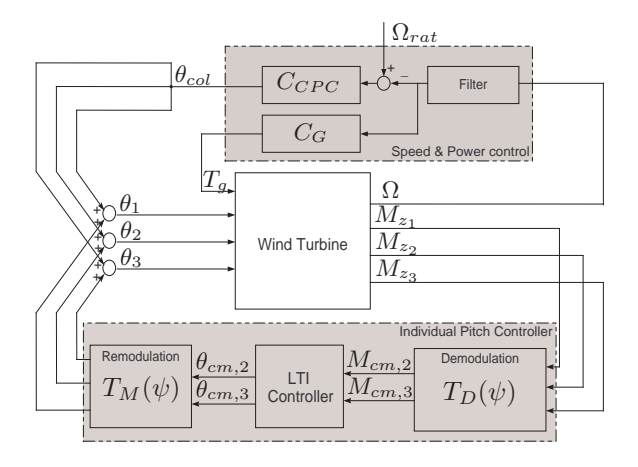


Figure 1: Wind turbine individual pitch control

IPC tilt and yaw-oriented pitch signals. This is performed in such a way that the IPC for blade load reduction uses only the actuation freedom that is not used up by the CPC algorithm and the IPC rotor balancing algorithm, achieving proper overall operation under the given blade pitch actuator limits.

The proposed IPC algorithms and anti-windup schemes are demonstrated on nonlinear simulations, consisting of a detailed structural dynamics model generated with the software Turbu [10], nonlinear blade momentum (BEM) aerodynamics (including dynamic wake effects and oblique inflow modeling), as well as realistic blade-element effective wind speeds, modeling wind shear, tower shadow, tilt and yaw misalignment, wind gusts and stochastic turbulence.

3 IPC for blade load reduction

This section discusses some IPC algorithms for blade load reduction, paying attention to both conventional I-type and advanced \mathcal{H}_{∞} control design. The starting point is the closed-loop interconnection, depicted on Figure 1, where C_{CPC} denotes the CPC algorithm, and C_G is the generator torque controller. The design of these basic controllers, C_{CPC} and C_G , falls outside the scope of this paper. For an overview of basic wind turbine control, refer to [2, 9].

The IPC controller for blade load reduction can be based on different measurements, though in this paper we will assume the availability blade root bending moments measurements since these are common in modern wind turbines. The use of other measurements (e.g. moments at the shaft or at the yaw bearing) is straightforward. Suppose the following linear parameter varying model describes the relevant dynamics of the wind turbine (possibly including the basic controllers C_{CPC} and C_G) from the three blade pitch angles θ_i , and axial blade effective wind speeds w_i , to the three flapwise blade root bending moments

$$M_{z_i}$$
, $i = 1, 2, 3$

where ψ is the rotor azimuth angle,

$$M_{z} = \begin{bmatrix} M_{z_{1}}(t) & M_{z_{2}}(t) & M_{z_{3}}(t) \end{bmatrix}^{T},$$

$$\theta = \begin{bmatrix} \theta_{1}(t) & \theta_{2}(t) & \theta_{3}(t) \end{bmatrix}^{T},$$

$$w = \begin{bmatrix} w_{1}(t) & w_{2}(t) & w_{3}(t) \end{bmatrix}^{T}$$

and the parameter $p=\{\Omega,\theta_{col},w_{ax}\}$ defines the operating point of the turbine, depending on the rotor speed Ω , the collective blade pitch angle $\theta_{col}=\frac{1}{3}(\theta_1+\theta_2+\theta_3)$, and the driving torque effective wind speed $w_{dr}=\frac{1}{3}(w_1+w_2+w_3)$. Although not explicitly denoted in the model, the parameters $\psi=\psi(t)$ and p=p(t) are functions of time. The blade-effective wind speeds w_i are fictitious signals defined in such a way, that they approximate (in statistical sense) the effects of full 3D longitudinal turbulence on the driving moments of the three blades [12].

Notice that for a fixed operating point $p(t)=p^*$, above model represents a periodic system, which complicates the controller design process. However, by transforming the signals M_z , θ and w (and states x) to the fixed rotor reference frame, one can convert this model into an LTI system. This so-called Coleman transformation, is based on the matrix

$$T_D(\psi) = \begin{bmatrix} \frac{1}{3} & \frac{1}{3} & \frac{1}{3} \\ \frac{2}{3}\sin(\psi) & \frac{2}{3}\sin(\psi + \frac{2\pi}{3}) & \frac{2}{3}\sin(\psi + \frac{4\pi}{3}) \\ \frac{2}{3}\cos(\psi) & \frac{2}{3}\cos(\psi + \frac{2\pi}{3}) & \frac{2}{3}\cos(\psi + \frac{4\pi}{3}) \end{bmatrix}$$
 (2)

which is used to demodulate the signals defined in the rotating coordinate frame into non-rotating *multi*blade coordinates

$$\begin{bmatrix} M_{cm,1} & \theta_{cm,1} & w_{cm,1} \\ M_{cm,2} & \theta_{cm,2} & w_{cm,2} \\ M_{cm,3} & \theta_{cm,3} & w_{cm,3} \end{bmatrix} = T_D(\psi_k) \begin{bmatrix} M_{z,1} & \theta_1 & w_1 \\ M_{z,2} & \theta_2 & w_2 \\ M_{z,3} & \theta_3 & w_3 \end{bmatrix}.$$

It has been shown in [10, 11] that this transformation gives an LTI model in multi-blade coordinates

$$\dot{x}_{cm} = A_{cm}(p)x_{cm} + B_{cm}(p)\theta_{cm} + E_{cm}(p)w_{cm} M_{cm} = C_{cm}(p)x_{cm} + D_{cm}(p)\theta_{cm} + F_{cm}(p)w_{cm}$$
 (3)

which takes the form of an LTI for a fixed operating point (i.e. for fixed p), allowing the use of conventional control design techniques. The resulting IPC should should then be connected to the original system using the Coleman demodulation matrix (2) and its inverse:

$$T_M(\psi) = \begin{bmatrix} 1 & \sin(\psi) & \cos(\psi) \\ 1 & \sin(\psi + \frac{2\pi}{3}) & \cos(\psi + \frac{2\pi}{3}) \\ 1 & \sin(\psi + \frac{4\pi}{3}) & \cos(\psi + \frac{4\pi}{3}) \end{bmatrix}.$$

The first multi-blade coordinate represents averaging over the blades. In other words, $\theta_{cm,1} \equiv \theta_{col}$ is

the collective pitch angle, $w_{cm,1} \equiv w_{dr}$ is the rotoraveraged axial wind speed. By actuating $\theta_{cm,2}$ and $\theta_{cm,3}$, the IPC controller adds up deviations around the collective pitch angle θ_{col} , which is controlled by the CPC (see Figure 1). Moreover, it can be shown that the rotor tilt and yaw moments are approximately proportional to the second and third multi-blade coordinates of the blade root flapwise moments. More specifically, when the influence of tensile and shearing forces and pitch-wise moments in the hub center are neglected, $M_{tilt} = \frac{3}{2} M_{cm,2}$ and $M_{yaw} =$ $\frac{3}{2}M_{cm,3}$. For that reason, the second multi-blade components of the input signals, $\theta_{cm,2}$ and $w_{cm,2}$, are referred to as tilt-oriented components (having mostly effect on the rotor tilt moment), while the $\theta_{cm,3}$ and $w_{cm,3}$ are called *yaw-oriented* components.

Finally, it should be pointed out that, due to rotational wind field sampling, tower shadow, and wind shear, the original blade effective wind speeds w_i contain frequency components at multiples of the rotational frequency, i.e. 1p, 2p, etc. This results in similar (n.p)components in the blade root moments M_{z_i} . In multiblade coordinates, however, these n.p frequencies in w_i are demodulated into 3.n.p frequencies in $w_{cm.2}$ and $w_{cm,3}$, resulting in 3p, 6p, 9p, etc., components in $M_{cm,2}$ and $M_{cm,3}$. More specifically, 1p components in M_z are transformed into static 0p tilt and yaw moments, $\{2p,4p\}$ frequencies in M_z become 3p components in the fixed frame, $\{5p,7p\}$ are modulated to 6p, and so on. Interestingly, 3.n.p components in the flap moments cancel out and have no influence on the rotor moments. For more inside into the effects of the Coleman transformation, see [10].

3.1 I-compensator IPC design

As explained above, 1p blade load reduction can be achieved by means of reducing the static (0p) rotor moments $M_{cm,2}$ and $M_{cm,3}$. Due to the negligible coupling between these at low frequencies, a SISO approach with two simple I-compensators is sufficient:

$$\theta_{cm,2} = \frac{k_2}{s} F_{IPC}(s) M_{cm,2},
\theta_{cm,3} = \frac{k_3}{s} F_{IPC}(s) M_{cm,3},$$
(4)

where $F_{IPC}(s)$ is series of band-stop filters around the 3p and 6p frequencies that prevents unnecessary propagation of these components in M_{cm} into the multi-blade pitch angles. A filter at the first tower frequency might also be needed. At steady state, $\theta_{cm,2}$ and $\theta_{cm,3}$ will converge to some static values, which after modulation to rotating coordinates, yield cyclic variations of the three blade pitch angles around θ_{col} , shifted by 120° :

$$\theta_i = \theta_{col} + \sin(\psi + \frac{(i-1)2\pi}{2})\theta_{cm,2} + \cos(\psi + \frac{(i-1)2\pi}{2})\theta_{cm,3}$$

The gains k_2 and k_3 can be selected to achieve some desired gain margin m_g (e.g. $m_g=2$). The phase margin cannot be influenced with k_j . To this end, denote $T_j(s),\ j=2,3,$ as the transfer function from $\theta_{cm,j}$ to $M_{cm,j}$ in (3), and consider the open-loop transfer

 $L_j(s) = \frac{k_2}{s} F_{IPC}(s) T_j(s).$

Due to the lack of poles of L(s) in the open right-half plane, a standard Nyquist stability analysis can be applied to compute k_j , i.e. $k_j = \frac{1}{m_g |T_j(\omega_{180^o})|}$ where ω_{180^o} is such that $\angle(T_j(\omega_{180^o})) = 180^o$.

3.2 Advanced IPC design

Although the SISO IPC approach above works well in practice, its stability should be analyzed carefully due to the neglected coupling between the two considered channels. These limitations can be removed by using more complex control structures, based on modern multivariable control synthesis methods. In fact, modern control design can also be used to achieve mitigation of blade loads at frequencies higher than 1p (i.e. 2p and higher), although this will not be pursued in this paper. Higher harmonics control gives rise to 2p and higher components in the blade pitch angles θ_i , leading easily to unrealistic actuation demands.

The goal here is to design a stabilizing controller that minimizes the low frequency components of the rotor moments' signals $M_{cm,2}$ and $M_{cm,3}$. In order to achieve zero steady state rotor moments, an integral action will be included in the controller. Furthermore, as was also the case with the simple I-compensator above, the controller should not be active at the 3p, the 6p, and possibly the first tower frequency. In addition to that, no high frequency control activity is desired. To achieve these performance specifications, an \mathcal{H}_{∞} -optimal controller with integral action can be designed, based on the MIMO transfer function T_{23} from the external inputs $w_{cm,23} = [w_{cm,2}, w_{cm,3}]^T$ and control action $\theta_{cm,23} = [\theta_{cm,2},\theta_{cm,3}]^T$ to the rotor moments $M_{cm,23} = [M_{cm,2}, M_{cm,3}]^T$. Figure 2 provides an block-schematic view of the design model. In order to include integral action into the controller, the output of the system T_{23} is appended with integrators (one integrator per output), which integrated model is used for an optimal \mathcal{H}_{∞} controller design C_{IPC}^{∞} . The final controller is constructed by moving the integrators, used in the design model, to the inputs of the computed controller (see the area inside the dashed curve on Figure 2). In order to comply with the frequency domain design specifications, the controller C^{∞}_{IPC} is designed by minimizing the \mathcal{H}_{∞} norm of the closed-loop transfer from the external inputs $w_{cm,23}$ to the weighted integrated rotor moments and weighted control signals, as shown in Figure 2 (see the generalized output signal y). The weighting function W_u should be selected to punish

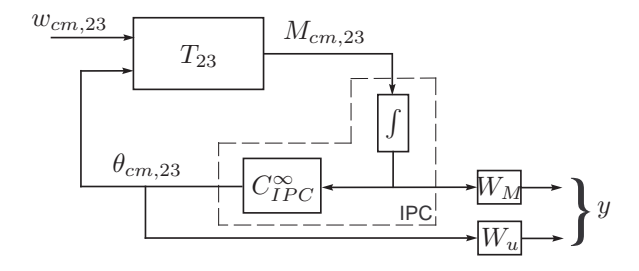


Figure 2: Block scheme for IPC design.

control activity at 3p, the 6p, first tower and higher frequencies. The weighting function W_M , on the other hand, needs to put a frequency domain weighting on the *integrated rotor moments*. As there is integral action in the controller anyway, the lower frequencies need not to be weighted additionally. Instead, W_M could put additional weighting on low frequencies as in [8].

The \mathcal{H}_{∞} controller is computed for the augmented model T_{23}^{aug}

$$\begin{bmatrix} y \\ M_{cm,23} \end{bmatrix} = T_{23}^{aug} \begin{bmatrix} w_{cm,23} \\ \theta_{cm,23} \end{bmatrix}, \ T_{23}^{aug} = \begin{bmatrix} \begin{bmatrix} 0 \ W_u(s) \end{bmatrix} \\ \frac{1}{s} W_M(s) T_{23}(s) \end{bmatrix}$$

via the following optimization problem [13]

$$C_{IPC}^{\infty} = \arg\min_{K} \|\mathcal{F}(T_{23}^{aug}(s), K(s))\|_{\infty},$$

where $\mathcal{F}(T_{23}^{aug}(s),K(s))$ denotes the closed-loop system, $\|\cdot\|_{\infty}$ denotes the \mathcal{H}_{∞} system norm, and wherein the optimization is defined over all controllers K(s) that have the same number of states as the augmented model $T_{23}^{aug}(s)$. Moving the integrators back to the controller results in the final IPC

$$C_{IPC}(s) = \begin{bmatrix} \frac{1}{s} & \\ \frac{1}{s} \end{bmatrix} C_{IPC}^{\infty}(s). \tag{5}$$

Since the \mathcal{H}_{∞} -controller order equals that of the augmented model, model reduction might be desirable.

3.3 Gain-scheduling

The IPC controllers, presented above, are based on a linearized turbine model, and will thus only achieve the specified design criteria at the working point where the model is valid. To achieve improved performance throughout the whole operation range of the turbine, a gain-scheduling approach can be used. As the IPC control is only to be active in above-rated wind conditions, the operating point is (statically) defined by θ_{col} . Hence, the gain of the IPC controller can be scheduled as a function of the collective pitch angle in such a way that the DC gain of the resulting open-loop transfer function remains constant. More specifically, suppose that the IPC controller $C_{IPC}(s)$ is designed based on the model $T_{23}(s)$, linearized around

some given operating point $p^* = \{\Omega_{rat}, \theta^*_{col}, w^*_{dr}\}$, defined by θ^*_{col} , and let $T^l_{23}(s)$, $l=1,2,\ldots,L$, denote linearizations of the dynamics from $\theta_{cm,23}$ to $M_{cm,23}$ around operating points with corresponding θ^l_{col} . By computing off-line the gain matrices

$$K_{qs}^{l} = T_{23}(0). (T_{23}^{l}(0))^{-1}, l = 1, 2, \dots, L,$$

one can gain-schedule the IPC controller based on the current collective pitch angle $\theta_{col}(t)$ as follows

$$j = \{l: l = 1, \dots, L, \ \theta_{col}^{l} \le \theta_{col}(t) \le \theta_{col}^{l+1}\},$$

$$\alpha(t) = \frac{\theta_{col} - \theta_{col}^{j}}{\theta^{j+1} - \theta_{col}^{j}},$$

$$\tilde{C}_{IPC}(s) = C_{IPC}(s) \left(\alpha(t)K_{gs}^{l+1} + (1 - \alpha(t))K_{gs}^{l}\right).$$

4 IPC rotor balancing

Rotor unbalance is caused by different aerodynamic conversion properties of the individual blades, and by mass distribution differences between the blades. Aerodynamic unbalance can be represented by adding extra terms ${\cal M}^{unb}_{z,i}$ to the nominal blade bending moments $M_{z,1}^{nom}$. The terms $M_{z,i}^{unb}$, i =1,2,3, have unequal non-zero mean value, that usually vary slowly. This unbalance causes nearly constant bending moment coordinates ${\cal M}_{sh,y}$ and ${\cal M}_{sh,z}$ on the rotor shaft. These induce variations in the tower-top moments M_{tlt} and M_{yw} around the 1pfrequency. These 1p variations can severely tamper with the IPC blade load reduction algorithm as they get demodulated into 2p pitch angle variations. This results in additional 2p loads in the flap moments and 3p loads in the tower top moments. The bending moment in the rotor shaft is the unbalanceidentifying quantity, and the compensation scheme below is based on the two shaft moment coordinates $M_{sh,y}$ and $M_{sh,z}$, cause by the blade flap moments:

$$\begin{bmatrix} M_{sh,y} \\ M_{sh,z} \end{bmatrix} = \underbrace{\begin{bmatrix} -\sin 0 & -\sin \frac{2}{3}\pi & -\sin \frac{4}{3}\pi \\ \cos 0 & \cos \frac{2}{3}\pi & \cos \frac{4}{3}\pi \end{bmatrix}}_{T_D^{sh}} \begin{bmatrix} M_{z,1} \\ M_{z,2} \\ M_{z,3} \end{bmatrix}.$$

Figure 3 shows the linearized closed-loop configuration for the IPC unbalance compensation loop (patent application filed, August 2008). The described method relies on shaft bending moment reconstruction from blade root flap moments. Another reconstruction option, not explored here due to space limitation, comprises the 1p modulation of measured tilt and/or yaw moment on the tower top.

The shaft moment coordinates $M_{sh,y}$ and $M_{sh,z}$ are first mapped to virtual pitch angle variations $\theta_{sh,y}$ and $\theta_{sh,z}$ along the shaft unit vectors, and then are transformed back to actual pitch angle variations

$$\begin{bmatrix} \theta_{bal,1} \\ \theta_{bal,2} \\ \theta_{bal,3} \end{bmatrix} = T_M^{sh} \begin{bmatrix} \theta_{sh,y} \\ \theta_{sh,z} \end{bmatrix}, \, T_M^{sh} = \frac{2}{3} \begin{bmatrix} -\sin 0 & \cos 0 \\ -\sin \frac{2}{3}\pi & \cos \frac{2}{3}\pi \\ -\sin \frac{4}{3}\pi & \cos \frac{4}{3}\pi \end{bmatrix},$$

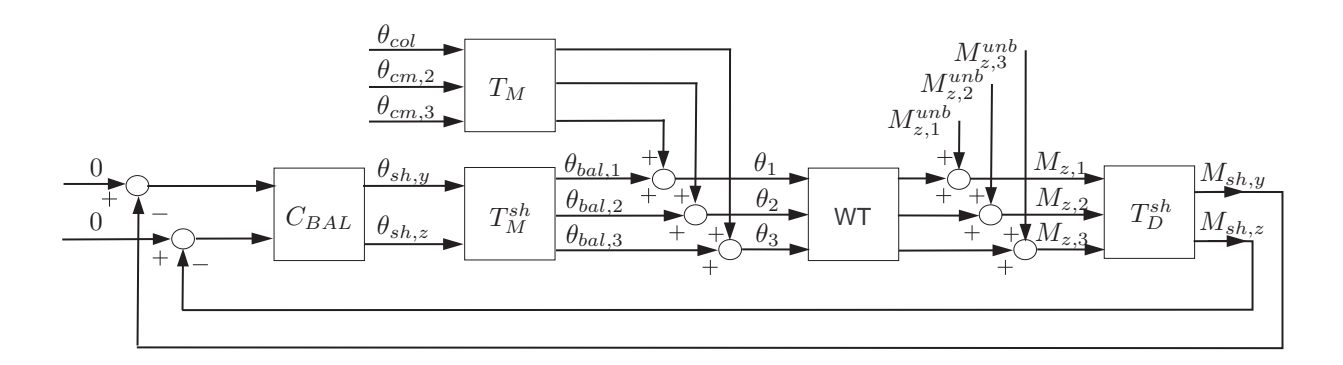


Figure 3: Rotor balancing IPC loop

which are added to the blade pitch angle variations from the CPC and IPC blade load reduction algorithm.

To design the balancing controller C_{BAL} , the wind turbine model from $\theta_{sh,y}$ and $\theta_{sh,z}$ to $M_{sh,y}$ and $M_{sh,z}$ is needed. The transfer from θ_i to $M_{z,i}$ is azimuth-dependent (see (1)). However, at low frequencies (typically below 0.1 Hz), the model can be approximated by a static, azimuth-independent and diagonal with the same gain for the two channels, i.e. $M_{sh,y} \approx k\theta_{sh,y}$ and $M_{sh,z} \approx k\theta_{sh,z}$. For such a low bandwidth, the phase is negligible. This allows the use of a simple controller structure, consisting of a first-order low-pass filter and integral action

$$\begin{bmatrix} \theta_{sh,y} \\ \theta_{sh,z} \end{bmatrix} = \frac{c_0}{s} \frac{1}{\tau s + 1} \begin{bmatrix} M_{sh,y} \\ M_{sh,z} \end{bmatrix},$$

giving closed-loop disturbance rejection

$$T_{sh}^{cl}(s) = \frac{1}{1 + k\frac{c_0}{s}\frac{1}{\tau s + 1}} = \frac{\frac{\tau s^2}{kc_0} + \frac{s}{kc_0}}{\frac{\tau s^2}{kc_0} + \frac{s}{kc_0} + 1}.$$

The controller parameters c_0 and τ are then chosen to yield a critically damped desired closed-loop system $(\beta=1)$ with given settling time T_{set} (e.g. 50 sec)

$$T_{sh}^{cl,desired}(s) = \frac{\frac{1}{\omega^2}s^2 + \frac{2\beta}{\omega_0}s}{\frac{1}{\omega^2}s^2 + \frac{2\beta}{\omega_0}s + 1},$$

with $\omega=\frac{4}{T_{set}\beta}.$ This is achieved with

$$\tau = \frac{T_{set}}{8}, \ c_0 = \frac{2}{k\beta^2 T_{set}}.$$

5 Anti-windup implementations

The pitch actuators in wind turbines have limits, and it is crucial that these limits are properly taken care of in the control algorithm. This is especially important for controllers with integral terms, as is the case with the discussed IPC algorithms above, as otherwise the well-known windup effect can occur, resulting in degraded performance or even instability. In this section, it is shown how anti-windup can be achieved

for the IPC algorithm. Implementation of anti-windup scheme for the CPC algorithm is just as important, but less involved and lies outside the scope of this paper.

Since the IPC algorithm is defined in the non-rotating reference frame, the original blade pitch angle, speed and acceleration limits need to be translated to multiblade coordinates before an anti-windup scheme can be applied. Moreover, in order to make sure that the IPC algorithm does not tamper with the CPC, it should only use the actuation freedom that is not used up by the CPC (and the rotor balancing IPC). In this way, proper simultaneous operation of all control algorithms is achieved, with priority to CPC.

The following positions, speeds and accelerations hard limits are considered for the blade actuators, i=1,2,3,

$$\begin{array}{l} \theta_{min} \leq \theta_{i} \leq \theta_{max}, \\ \dot{\theta}_{min} \leq \dot{\theta}_{i} \leq \dot{\theta}_{max}, \\ \ddot{\theta}_{min} \leq \ddot{\theta}_{i} \leq \ddot{\theta}_{max}, \end{array} \tag{6}$$

where the minimum and maximum values are assumed given. Part of this total actuation freedom is attributed to the basic CPC algorithm and the rotor balancing IPC, and it is assumed that the following limits are met at all time

$$\theta_{min} \leq \theta_{min}^{col} \leq \theta_{col} \leq \theta_{max}^{col} \leq \theta_{max},
\dot{\theta}_{min} < \dot{\theta}_{min}^{col} \leq \dot{\theta}_{col} \leq \dot{\theta}_{max}^{col} < \dot{\theta}_{max},
\ddot{\theta}_{min} < \ddot{\theta}_{col}^{col} \leq \ddot{\theta}_{col}^{col} < \ddot{\theta}_{max}^{col},$$
(7)

Notice that the speed and acceleration constraints for the CPC action are chosen strictly inside the actuator limits, hence always leaving some freedom for the IPC controller. For the pitch angle it is not always possible to select $\theta_{min} < \theta_{min}^{col}$ strictly, as would be the case when the lower pitch angle bound θ_{min} coincides with the working position at below-rated conditions (which should be reachable by θ_{col}).

5.1 Multi-blade pitch limits

Defining $\psi_i \doteq \psi_k + \frac{2\pi(i-1)}{3}$ as the azimuth angle of blade i, we can then write

$$\theta_i = \theta_{col} + \sin(\psi_i)\theta_{cm,2} + \cos(\psi_i)\theta_{cm,3}, \ i = 1, 2, 3.$$

Clearly, the IPC actions $\theta_{cm,2}$ and $\theta_{cm,3}$ have effect on all three blade angles, speeds and accelerations. Still, they should not lead to the original actuator limits (6) getting exceeded. To achieve this, limits on the IPC actions $\theta_{cm,2}$ and $\theta_{cm,3}$ will be derived for which (6) remain valid. It is desirable that these limits do not (explicitly) depend on the rotor azimuth ψ_k . To this end, the remaining freedom in the actuators after the CPC controller will be distributed among the two IPC controls. Define

$$\begin{array}{ll} \theta^{rest} \doteq \max\{0, \min\{\theta_{max} - \theta_{col}, \theta_{col} - \theta_{min}\}\}, \\ \dot{\theta}^{rest} \doteq \max\{0, \min\{\dot{\theta}_{max} - \dot{\theta}_{col}, \dot{\theta}_{col} - \dot{\theta}_{min}\}\}, \\ \ddot{\theta}^{rest} \doteq \max\{0, \min\{\ddot{\theta}_{max} - \ddot{\theta}_{col}, \ddot{\theta}_{col} - \ddot{\theta}_{min}\}\}, \end{array}$$

where the current collective pitch speed $\dot{\theta}_{col}$ and acceleration $\ddot{\theta}_{col}$ should be substituted by their finite difference approximations.

Denoting

$$J(\psi, \theta_{cm,2}, \theta_{cm,3}) \doteq \sin(\psi)\theta_{cm,2} + \cos(\psi)\theta_{cm,3}$$

the purpose of this section is to derive limits on the IPC angles $\theta_{cm,2}$ and $\theta_{cm,3}$, as well as on their speeds and accelerations, such that *for any* ψ the following inequalities are satisfied

$$\begin{vmatrix}
J(\psi, \theta_{cm,2}, \theta_{cm,3}) \\
\dot{J}(\psi, \theta_{cm,2}, \theta_{cm,3}) \\
\ddot{J}(\psi, \theta_{cm,2}, \theta_{cm,3})
\end{vmatrix} \le \begin{bmatrix} \theta^{rest} \\ \dot{\theta}^{rest} \\ \ddot{\theta}^{rest} \end{bmatrix}.$$
(8)

To keep the problem tractable, we distribute the available freedom between the two IPC controls. In doing this, however, we do not use a constant factor, but rather look at the "activity" of the two signals. If, for instance, there is large rotor yaw misalignment, this will give raise to a large rotor tilt moment, so that $\theta_{cm,2}$ will need to get larger to compensate this, while at the same time the yaw-oriented component $\theta_{cm,3}$ might be negligible. Hence, we will distribute θ^{rest} (and, of course, $\dot{\theta}^{rest}$ and $\ddot{\theta}^{rest}$) by looking at the values of $\theta_{cm,2}^{unlim}$ and $\theta_{cm,3}^{unlim}$, required by the IPC controller before applying any limits on them, so that the signal that is larger in absolute value gets more freedom than the "less active" signal. This idea is used in the following to derive the limits on the IPC signals $\theta_{cm,j}$, $\dot{\theta}_{cm,j}, \ddot{\theta}_{cm,j}, j=2,3.$

Position limit: $J(\psi, \theta_{cm,2}, \theta_{cm,3}) \leq \theta^{rest}$

To begin with, consider the first constraint in (8), and suppose that $\alpha_2>0$ and $\alpha_3>0$ are two given scalars, such that

$$|\theta_{cm,j}| \le \alpha_j \theta^{rest}, \ j = \{2,3\}. \tag{9}$$

Then it holds that.

$$[\max_{\psi} J(\psi, \theta_{cm,2}, \theta_{cm,3}) \equiv \sqrt{(\theta_{cm,2}^2 + \theta_{cm,3}^2)}]$$

$$\leq \theta^{rest} \sqrt{\alpha_2^2 + \alpha_3^2}.$$

Since we need to make sure that $J(\psi,\theta_{cm,2},\theta_{cm,3}) \leq \theta^{rest}$ for all ψ , the scalars α_2 and α_3 should be such that $\alpha_2^2 + \alpha_3^2 = 1$. Moreover, from the discussion above, we would like that the ratio between the limits for $\theta_{cm,2}$ and $\theta_{cm,3}$ is proportional to the ratio between $|\theta_{cm,2}^{unlim}|$ and $|\theta_{cm,3}^{unlim}|$ (i.e. the ratio between the IPC controller outputs before applying any limits). This implies that

$$\frac{\alpha_2}{\alpha_3} = \frac{|\theta_{cm,2}^{unlim}|}{|\theta_{cm,3}^{unlim}|}.$$

Solving this equality together with $\alpha_2^2 + \alpha_3^2 = 1$ gives

$$\alpha_j \doteq \frac{|\theta_{cm,j}^{unlim}|}{\sqrt{(\theta_{cm,2}^{unlim})^2 + (\theta_{cm,3}^{unlim})^2}}, \ j = \{2,3\}, \quad (10)$$

which, with (9), ensures the first inequality in (8).

Speed limit:
$$\dot{J}(\psi, \theta_{cm,2}, \theta_{cm,3}) \leq \dot{\theta}^{rest}$$

Consider the speed constraint in (8), written as

$$\begin{split} \dot{J}(\psi,\theta_{cm,2},\theta_{cm,3}) &= \dot{J}_{2}(\psi,\theta_{cm,2}) + \dot{J}_{3}(\psi,\theta_{cm,3}), \\ \dot{J}_{2}(\psi,\theta_{cm,2}) &\doteq \Omega \cos(\psi)\theta_{cm,2} + \sin(\psi)\dot{\theta}_{cm,2}, \\ \dot{J}_{3}(\psi,\theta_{cm,3}) &\doteq -\Omega \sin(\psi)\theta_{cm,3} + \cos(\psi)\dot{\theta}_{cm,3}. \end{split}$$

In this case, similarly to what we did above for the position limit, we distribute $\dot{\theta}^{rest}$ between $\dot{J}_2(\psi,\theta_{cm,2})$ and $\dot{J}_3(\psi,\theta_{cm,3})$ by using β_2 and β_3 , such that

$$|\dot{J}_i(\psi, \theta_{cm,i})| \le \beta_i \dot{\theta}^{rest}, \ j = \{2, 3\}, \tag{11}$$

implying

$$\max_{\psi} \dot{J}(\psi, \theta_{cm,2}, \theta_{cm,3}) = (\beta_2 + \beta_3) \dot{\theta}^{rest},$$

so $\beta_2 + \beta_3 = 1$ must hold. This, together with

$$\frac{\beta_2}{\beta_3} = \frac{|\theta_{cm,2}^{unlim}|}{|\theta_{cm,3}^{unlim}|},$$

gives

$$\beta_j \doteq \frac{\left|\theta_{cm,j}^{unlim}\right|}{\left|\theta_{cm,2}^{unlim}\right| + \left|\theta_{cm,3}^{unlim}\right|}, \ j = \{2, 3\}. \tag{12}$$

It remains to rewrite (11) in terms of $\theta_{cm,j}$ and $\dot{\theta}_{cm,j}$. Here, there is another degree of freedom in the choice of distributing $\beta_j \dot{\theta}^{rest}$ over the position $\theta_{cm,j}$ and speed $\dot{\theta}_{cm,j}$. For that purpose, we choose factors $\gamma_{pos}>0$ and $\gamma_{spd}>0$ such that for some $\dot{\theta}_j^{rest}>0$ (derived below) we require that

$$\begin{aligned} |\dot{\theta}_{cm,j}| &\leq \gamma_{pos} \dot{\theta}_{j}^{rest}, \\ |\dot{\theta}_{cm,j}| &\leq \gamma_{spd} \dot{\theta}_{i}^{rest}. \end{aligned} \tag{13}$$

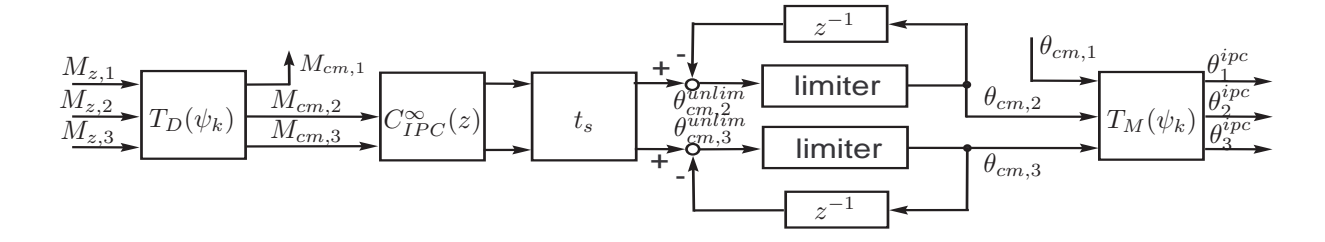


Figure 4: IPC anti-windup scheme

To derive an expression for $\dot{\theta}_i^{rest}$, note that

$$\max_{\psi} \dot{J}_{j}(\psi, \theta_{cm,j}) = \sqrt{(\Omega \theta_{cm,j})^{2} + \dot{\theta}_{cm,j}^{2}} \\ \leq \dot{\theta}_{j}^{rest} \sqrt{\gamma_{pos}^{2} \Omega^{2} + \gamma_{spd}^{2}}.$$

Hence, inequality (11) will be satisfied for

$$\dot{\theta}_{j}^{rest} = \frac{\beta_{j} \dot{\theta}^{rest}}{\sqrt{\gamma_{pos}^{2} \Omega^{2} + \gamma_{spd}^{2}}},\tag{14}$$

with β_i defined in (12).

Acceleration limit: $\ddot{J}(\psi, \theta_{cm,2}, \theta_{cm,3}) \leq \ddot{\theta}^{rest}$

For the acceleration limit in (8), we can write

$$\begin{split} \ddot{J}(\psi,\theta_{cm,2},\theta_{cm,3}) &= \ddot{J}_{2}(\psi,\theta_{cm,2}) + \ddot{J}_{3}(\psi,\theta_{cm,3}), \\ \ddot{J}_{2}(\psi,\theta_{cm,2}) &\doteq (\ddot{\theta}_{cm,2} - \Omega^{2}\theta_{cm,2})\sin(\psi) \\ &+ (2\Omega\dot{\theta}_{cm,2} + \dot{\Omega}\theta_{cm,2})\cos(\psi), \\ \ddot{J}_{3}(\psi,\theta_{cm,3}) &\doteq (\ddot{\theta}_{cm,3} - \Omega^{2}\theta_{cm,3})\cos(\psi) \\ &- (2\Omega\dot{\theta}_{cm,3} + \dot{\Omega}\theta_{cm,3})\sin(\psi). \end{split}$$

Similarly to the speed limit case, we distribute $\ddot{\theta}^{rest}$ between $\ddot{J}_2(\psi, \theta_{cm,2})$ and $\ddot{J}_3(\psi, \theta_{cm,3})$ by using the same scalars β_2 and β_3 as in (12)

$$|\ddot{J}_j(\psi, \theta_{cm,j})| \le \beta_j \ddot{\theta}^{rest}, \ j = \{2, 3\}, \tag{15}$$

since then we get $\max_{\psi} \ddot{J}(\psi,\theta_{cm,2},\theta_{cm,3}) = \ddot{\theta}^{rest}$, as required in (8). Now we have even more freedom than in the speed limit case above, since we have to distribute $\beta_j \ddot{\theta}^{rest}$ between three components: the position $\theta_{cm,j}$, the speed $\dot{\theta}_{cm,j}$ and the acceleration $\ddot{\theta}_{cm,j}$. To do this, we choose, in addition to the already chosen factors γ_{pos} and γ_{spd} , a third factor $\gamma_{acc} > 0$, and we impose the following constraints for some $\ddot{\theta}_{r}^{rest} > 0$ that is yet to be derived

$$\begin{aligned} |\theta_{cm,j}| &\leq \gamma_{pos} \ddot{\theta}_{j}^{rest}, \\ |\dot{\theta}_{cm,j}| &\leq \gamma_{spd} \ddot{\theta}_{j}^{rest}, \\ |\ddot{\theta}_{cm,j}| &\leq \gamma_{acc} \ddot{\theta}_{j}^{rest}. \end{aligned}$$
(16)

Under these constraints we have

$$\max_{\psi} \ddot{J}_{j}(\psi, \theta_{cm,j})$$

$$= \sqrt{(\ddot{\theta}_{cm,j} - \Omega^{2}\theta_{cm,j})^{2} + (2\Omega\dot{\theta}_{cm,j} + \dot{\Omega}\theta_{cm,j})^{2}}$$

$$\leq \ddot{\theta}_{j}^{rest} \sqrt{(\gamma_{acc} + \Omega^{2}\gamma_{pos})^{2} + (2\Omega\gamma_{spd} + \dot{\Omega}\gamma_{pos})^{2}}$$

Inequality (15) will then be satisfied under constraints (16) with

$$\ddot{\theta}_{j}^{rest} = \frac{\beta_{j}\ddot{\theta}^{rest}}{\sqrt{(\gamma_{acc} + \Omega^{2}\gamma_{pos})^{2} + (2\Omega\gamma_{spd} + \dot{\Omega}\gamma_{pos})^{2}}}$$
(17)

and β_i defined in (12).

5.2 Anti-windup scheme

To summarize, the final limits on the IPC actions in multi-blades coordinates are obtained by combining (9),(13),(16) together with the scalings (10),(12),(14),(17). In order to describe how the anti-windup scheme should finally be implemented into the wind turbine controller, we assume below that the IPC controller is discretized with sampling period of t_s seconds, and will approximate the speeds and accelerations with finite differences. At time instant k, the following constraints should then be active

$$|\theta_{cm,j}(k)| \leq \min \left\{ \alpha_{j} \theta^{rest}, \gamma_{pos} \dot{\theta}_{j}^{rest}, \gamma_{pos} \ddot{\theta}_{j}^{rest} \right\} (18)$$

$$|\theta_{cm,j}(k) - \theta_{cm,j}(k-1)| \leq \min \left\{ t_{s} \gamma_{spd} \dot{\theta}_{j}^{rest}, t_{s} \gamma_{spd} \ddot{\theta}_{j}^{rest} \right\} (19)$$

$$|\theta_{cm,j}(k) - 2\theta_{cm,j}(k-1) + \theta_{cm,j}(k-2)| \leq t_{s}^{2} \gamma_{acc} \ddot{\theta}_{j}^{rest} (20)$$

Notice, that both IPC controllers (4) and (5), discretized with sampling period t_s , have the same general representation

$$C_{IPC}(z) = \begin{bmatrix} \frac{t_s}{1-z^{-1}} \\ \frac{t_s}{1-z^{-1}} \end{bmatrix} C_{IPC}^{\infty}(z),$$

consisting of integrators at the output, followed by a transfer function (filter). As discussed in [6], in order to achieve an anti-windup mechanism one needs to make sure that the integrator states are driven by the actual (constrained) inputs $\theta_{cm,2}$ and $\theta_{cm,3}$. This can be achieved easily by implementing the integrators by using one sample delay feedback around the limiters, as shown in Figure 4. The two limiters, having the same structure, but realizing the bounds in (18)-(20) for $j = \{2,3\}$, are shown in Figure 5.

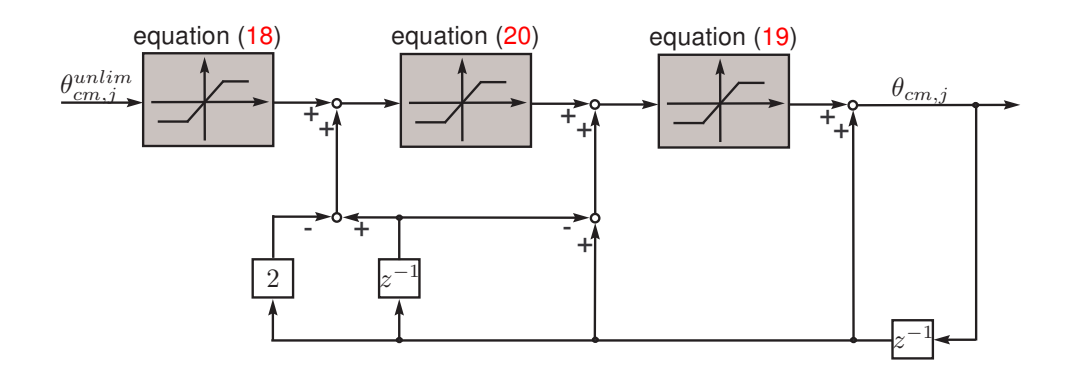


Figure 5: IPC pitch limiter realization

5.3 Limits under blade speed control

Above, the discussion was focused on the blade pitch angles θ_i being the control signals. In practice, however, it is sometimes the case that the pitch speeds θ_i are the control variables, which leads to controller structures that contain no integrators. Indeed, an I-compensator for IPC will take the form of a P-compensator when the pitch speed is used. For P and PD controllers, windup is not an issue, so the anti-windup scheme, presented in section 5.2, will not be an issue. In this case, the limiter block can be positioned simply after the controller. However, the limiter will have a different structure than the one in Figure 5. The reason for this is that the controller does not output a position signal. In order to incorporate position constraints, actual blade angle measurements $\theta_i^{meas}(k)$ are necessary, which we again transform to multi-blade coordinates $\theta_{cm,j}^{meas}$ using the Coleman demodulation matrix $T_D(\psi)$ (2). The corresponding limiter scheme is depicted on Figure 6.

6 Nonlinear simulation study

In this section, the methods, discussed above are demonstrated via realistic nonlinear wind turbine simulations. The simulation model is briefly described in the next subsection, after which the results of different simulations are presented, aiming to illustrate the influence of IPC on the blade loads, the operation of the rotor balancing IPC algorithm in case of blade pitch unbalance, as well as the effect of the proposed

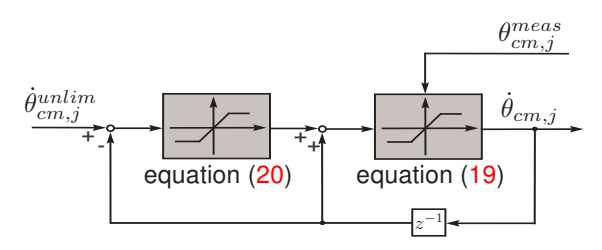


Figure 6: Limiter realization under speed control

IPC anti-windup scheme.

6.1 Simulation model

The nonlinear wind turbine simulation model, used for generating the results in this paper, consists of the following components:

- 156-th order linearized structural dynamics model (SDM), obtained using the software Turbu [11]. A multi-body approach has been used to obtain this detailed SDM. The multi-body model has 14 elements per blade and 15 elements for the tower, with each element having 5 degrees of freedom. There are 6 degrees of freedom in the rotor shaft, and 12 for the pitch-servo actuation system. A linearization is computed for an aerodynamic equilibrium state at a mean wind speed of 15 m/s, rotor speed of approx. 17,7 rpm and blade pitch angle of 7,24 deg.
- o nonlinear aerodynamic conversion module (ADM), based on blade element momentum (BEM) theory, including dynamic wake effects, the effects of oblique inflow on the axial induction speed, and angle of attack correction due to rotor coning. The ADM computes forces and torques per blade elements, which are used to load the SDM. See [8] for details on the ADM.
- o basic CPC controller, regulating the filtered generator speed at its rated level (when operating at above-rated conditions). It consisting of a PI-controller in series with low-pass filter at the 3p blade frequency, notch filter at the first tower sidewards frequency, and notch filter at the first collective lead-lag frequency. An anti-windup scheme is implemented for this CPC controller to guarantee that constraints (7) are satisfied.
- o nonlinear generator torque controller based on static optimal- λ QN-curve at below rated conditions and *constant power* production above-rated, operating on the filtered generator speed signal (same three filters used as in pitch controller).
- \circ IPC: the advanced \mathcal{H}_{∞} controller does not perform significantly better than the conventional I-compensator, the later is used in the simulations

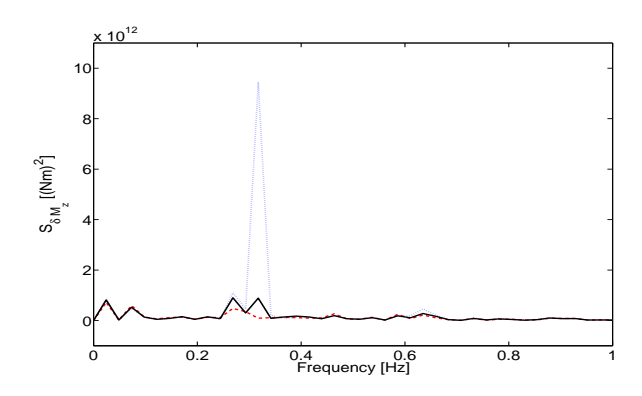


Figure 7: Blade 1 flapwise moment spectrum for Case 1 (dotted), Case 2 (dashed), Case 3 (solid)

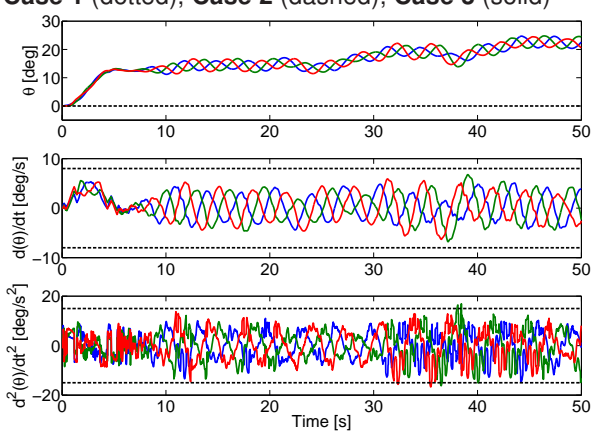


Figure 8: Pitch angle, speed and acceleration reference anti-windup IPC for blade load reduction

reported here. The gain scheduling is done based on support points corresponding to mean wind speeds, equally spaced over intervals of 1 m/s.

 realistic blade effective wind speed signals are generated based on the helix approximation concept, as proposed in [8, App. C], including both deterministic terms for wind shear, tower shadow, tilt and yaw misalignment, wind gust, and a stochastic term for blade-effective turbulence. The mean wind speed, used in the simulations, is 20 m/s, reaching the rotor at oblique inflow angle of 10 degrees.

6.2 IPC for blade load reduction

To evaluate the performance of the proposed advanced IPC scheme for 1p blade load reduction, three simulations have been performed:

- o Case 1: without IPC control.
- Case 2: with IPC for blade load reduction, no pitch limits,
- Case 3: with IPC for blade load reduction, pitch limits included.

The resulting blade 1 flapwise root bending moment spectrum for the three cases are plotted in Figure 7. Clearly, a significant reduction of blade loads is achieved around the 1p frequency, both without and with pitch limits (anti-windup), although the later case

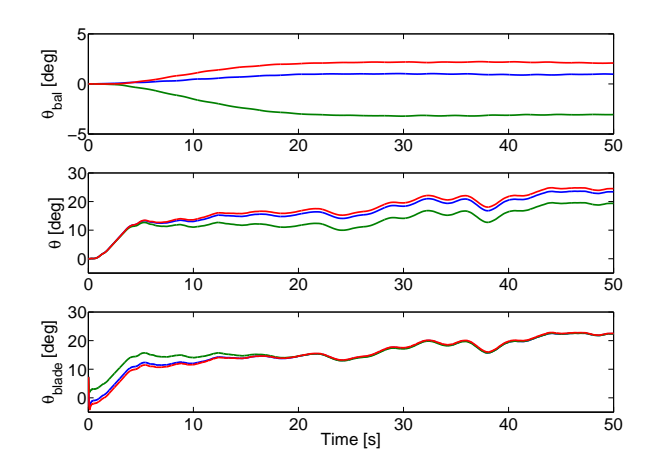


Figure 9: Pitch angles from rotor-balancing IPC (top), total pitch angle reference sent to pitch actuators (middle), actual pitch setting angles (bottom)

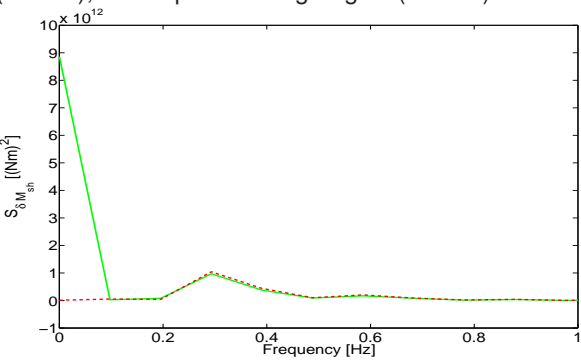


Figure 10: Rotor shaft moment spectrum for **Case 4** (solid) and **Case 5** (dashed)

gives slightly less reduction, as expected. Figure 8 shows the pitch angle, speed and acceleration under Case 3, together with their limits, given in Table 1.

6.3 Rotor balancing

For demonstrating the rotor balancing algorithm, two simulations are used:

- o Case 4: no rotor balancing, no IPC, no pitch limits
- o Case 5: rotor balancing, no IPC, no pitch limits

In both Cases 4 and 5, aerodynamic unbalance is introduced by adding offsets to the three blade pitch angles of respectively -1, 3 and -2 degrees. From the top plot in Figure 9 it can be seen that the IPC rotor balancing algorithm cancel the rotor unbalance by pitching the blades to values opposite to the modeled offsets, which is done by nearly zeroing the slowly varying mean shaft moment (see Figure 10).

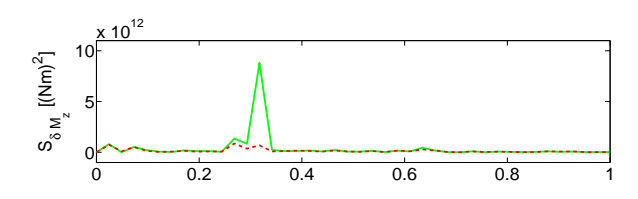
6.4 Blade load reduction and balancing

Finally, a simulation is performed under aerodynamic rotor unbalance (as in Cases 4 and 5) and with both IPC controllers activated, i.e.

Case 6: rotor balancing and IPC for blade load reduction, pitch limits included.

parameter	θ_{min}	θ_{max}	$\dot{\theta}_{min}$	$\dot{\theta}_{max}$	$\ddot{\theta}_{min}$	$\ddot{\theta}_{max}$	θ_{min}^{col}	θ_{max}^{col}	$\dot{ heta}_{min}^{col}$	$\dot{ heta}_{max}^{col}$	$\ddot{\theta}_{min}^{col}$	$\ddot{\theta}_{max}^{col}$	γ_{pos}	γ_{spd}	γ_{acc}
value	0	85	-8	8	-15	15	0	85	-4	4	-5	5	4	1	8
dimension	0	0	$^{o}/s$	$^{o}/s$	$^{o}/s^{2}$	$^{o}/s^{2}$	0	0	$^{o}/s$	$^{o}/s$	$^{o}/s^{2}$	$^{o}/s^{2}$	-	-	-

Table 1: Numerical values of the algorithm parameters



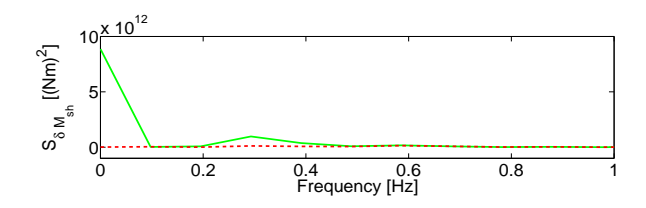


Figure 11: Blade root flapwise moment (top) and shaft moment (bottom) under Case 4 (solid) and Case 6 (dashed)

This simulation case is compared to Case 4 (aerodynamic unbalance, no IPC), and the results are presented in Figure 11. Clearly, the oblique wind inflow results in a large 1p blade root moment, which is excellently mitigated by the IPC for blade load reduction (top plot), while the large static shaft moment created by the aerodynamic unbalance is reduced by the rotor balancing scheme by pitching the blades to angles opposite to the simulated offsets (bottom plot). Although not plotted due to space limitation, the antiwindup implementation ensures that the blade pitch angles, speeds and accelerations remain within the specified limits.

7 Acknowledgements

SenterNovem is acknowledged for supporting this work in the project "Sustainable Control, a new Approach to Operate Wind Turbines (SUSCON)", under grant EOSLT02013 in the EOS research programme.

8 Conclusions

This paper discusses different approaches for fatigue load reduction in wind turbines based on IPC algorithms. Besides the usual IPC aim for 1p blade load reduction, a novel method for rotor balancing IPC is presented that works by mitigating static shaft moments. Special attention is paid on gain-scheduling, dealing with actuator constraints and preventing windup. Detailed realistic nonlinear simulations are used to validate the methods, paving the way towards practical application.

References

- E. Bossanyi. Developments in individual blade pitch control. In *Proceedings of "the Science of Making Torque from Wind" Conference*, pages 486–497, 2004.
- [2] E.A. Bossanyi. The design of closed loop controllers for wind turbines. Wind Energy, 3:149–163, 2000.
- [3] E.A. Bossanyi. Individual blade pitch control for load reduction. *Wind Energy*, 6:1919–128, 2003.
- [4] E.A. Bossanyi. Wind turbine control for load reduction. *Wind Energy*, 6:229–244, 2003.
- [5] M. Geyler and P. Caselitz. Individual blade pitch control design for load reduction on large wind turbines. In *Proceeding of the European Wind Energy Conference*, pages 82–86, Milan, Italy, 2007
- [6] G. Goodwin, F. Graebe, and M. Salgado. Control System Design. Prentice Hall, Upper Saddle River, New Jersey, 2001.
- [7] B. S. Kallesœ. A low-order model for analysing effects of blade fatigue load control. *Wind Energy*, 9:421–436, 2006.
- [8] S. Kanev and T. van Engelen. Wind turbine extreme gust control. Technical Report ECN-E-08-069, ECN Wind Energy, 2008. http://www.ecn.nl/publicaties/ default.aspx?nr=ECN-E--08-069.
- [9] E.L. van der Hooft, P. Schaak, and T.G. van Engelen. Wind turbine control algorithms. Technical Report ECN-C-03-111, Energy Research Center of the Netherlands (ECN), 2003. DOWEC-F1W1-EH-03-094/0.
- [10] T. van Engelen. Design model and load reduction assessment for multi-rotational mode individual pitch control (higher harmonics control). In *Proceedings of the European Wind Energy Conference*, Athens, Greece, 2006. http://www.ecn.nl/publicaties/default.aspx?nr=ECN-RX--06-068.
- [11] T. van Engelen. Control design based on aerohydro-servo-elastic linear models from TURBU (ECN). In *Proceeding of the European Wind En*ergy Conference, Milan, Italy, 2007.
- [12] T. van Engelen and P. Schaak. Oblique inflow model for assessing wind turbine controllers. In Proceedings of the 2nd Conference on The Science of Making Torque From Wind, Denmark, 2007.
- [13] K. Zhou and J. Doyle. *Essentials of Robust Control*. Prentice-Hall, 1998.